# Figures of merit and constraints from testing general relativity using the latest cosmological data sets including refined COSMOS 3D weak lensing

Jason N. Dossett, Jacob Moldenhauer, and Mustapha Ishak

Phys. Rev. D **84**, 023012 — Published 26 July 2011

DOI: 10.1103/PhysRevD.84.023012

# Figures of merit and constraints from testing General Relativity using the latest cosmological datasets including refined COSMOS 3D weak lensing

Jason N. Dossett*, Jacob Moldenhauer†, Mustapha Ishak‡
*Department of Physics, The University of Texas at Dallas, Richardson, TX 75083, USA;*

We use cosmological constraints from current datasets and a figure of merit approach (FoM) in order to probe any deviations from general relativity at cosmological scales. The FoM approach is used to study and compare the constraining power of various combinations of datasets on the modified gravity (MG) parameters. We use the recently refined HST-COSMOS weak lensing tomography data, the ISW-galaxy cross correlations from 2MASS and SDSS LRG galaxy surveys, the matter-power spectrum from SDSS-DR7 (MPK), the WMAP7 temperature and polarization spectra, the BAO from 2DF and SDSS-DR7, and the Union2 compilation of type Ia supernovae, in addition to other bounds from Hubble parameter measurements and Big Bang Nucleosynthesis. We use three parameterizations of MG parameters that enter the perturbed field equations. In order to allow for variations of the parameters with the redshift and scale, the first two parameterizations use recently suggested functional forms while the third is based on binning methods. Using the first parameterization, we find that the CMB+ISW+WL combination provides the strongest constraints on the MG parameters followed by CMB+WL or CMB+MPK+ISW. Using the second parameterization or the binning methods, we find that the combination CMB+MPK+ISW consistently provides some of the strongest constraints. This shows that the constraints are parameterization dependent. We find that adding up current datasets does not improve consistently the uncertainties on MG parameters due to tensions between the best fit MG parameters preferred by different datasets. Furthermore, some functional forms imposed by the parameterizations can lead to an exacerbation of these tensions. Next, unlike some studies that used the CFHTLS lensing data, we do not find any deviation from GR using the refined HST-COSMOS data, confirming previous claims in those studies that their result may have been due to some systematic effect. Finally, for all the parameterizations and binning methods used, we find that the values corresponding to general relativity are within the 95% confidence level contours for all data set combinations.

PACS numbers: 95.36.+x,98.80.Es,98.62.Sb

## I. INTRODUCTION

One of the routes to understanding the origin of cosmic acceleration is by testing whether the acceleration is due to a dark energy component pervading the universe or some modification to general relativity (GR) at cosmological scales of distances. The study of the growth rate of large scale structure can help to make such a distinction and has been the subject of a number of analyses in the literature. Some first papers (see for example [1–4]) studied inconsistency between constraints on parameters from the growth rate and constraints from the expansion history to detect deviations from GR using observations. These were followed by another approach (see for example [5–46]) that based their analysis on various growth parameters that take distinctive values for distinct gravity theories. For example, in GR, some parameters take the unity value and deviation from it would indicate deviations from GR. It is worth mentioning that some useful pioneering work on the growth rate parameterization in for example [47–50] had been done for a purpose other than seeking to distinguish between dark energy and modified gravity (MG). Finally, it is informative to refer to all the early work about post-GR parameterizations that had been proposed to test deviations from GR at the level of solar system tests, for example see [51, 52] and references therein.

Recently, some studies used current available datasets in order to constrain the MG parameters and to see if there is an indication of any deviation from GR but in vain so far [53–59].

In this paper, we calculate and compare constraints and figures of merit (FoM) on MG parameters based on functional forms or binning methods, using combined datasets of baryon acoustic oscillations (BAO) measurements from Two-Degree Field (2dF) and DR7 Sloan Digital Sky (SDSS) surveys [60, 61], the WMAP 7-year (WMAP7) CMB temperature (TT) and polarization (TE) spectra [62], and the supernovae Union2 compilation, which includes the 557 Type Ia SNe of the Supernovae Cosmology Project (SCP) [63], and references of other compiled supernovae therein, the matter power spectrum (MPK) from SDSS DR7 [60], the Integrated Sachs Wolfe (ISW)-galaxy cross

* Electronic address: jnd041000@utdallas.edu
† Electronic address: jam042100@utdallas.edu
‡ Electronic address: mishak@utdallas.edu

correlations with the 2MASS and SDSS LRG galaxy surveys [64, 65], and the recently refined Hubble Space Telescope (HST) Cosmic Evolution Survey (COSMOS) weak lensing tomography analysis in [66].

## II. METHODOLOGY

### A. Unmodified Growth Equations

For convenience, we will work in the conformal Newtonian Gauge, where the perturbed Friedmann-Lemaitre-Robertson-Walker metric is written as:

$$ds^2 = a(\tau)^2[-(1+2\psi)d\tau^2 + (1-2\phi)dx^i dx_i], \tag{1}$$

where $a(\tau)$ is the scale factor normalized to one today, the $x_i$'s are the comoving coordinates, and $\tau$ is conformal time. $\phi$ and $\psi$ are scalar potentials describing the scalar mode of the metric perturbations.

We can get two very useful equations that describe the evolution of the scalar potentials by using the first-order perturbed Einstein equations working in Fourier k-space. Combining the time-time and time-space equations gives the Poisson equation. Taking the traceless, space-space component of these equations lets us relate the two potentials. Respectively, we have:

$$k^2\phi = -4\pi G a^2 \sum_i \rho_i \Delta_i \tag{2}$$

$$k^2(\psi - \phi) = -12\pi G a^2 \sum_i \rho_i (1+w_i)\frac{\pi_i}{2}, \tag{3}$$

where $\rho_i$ and $\pi_i$ are the density and the anisotropic stress, respectively, for matter species, $i$. $\Delta_i$ is the gauge-invariant, rest-frame overdensity for matter species, $i$, the evolution of which describes the growth of inhomogeneities. It is defined by:

$$\Delta_i = \delta_i + 3\mathcal{H}\frac{q_i}{k}, \tag{4}$$

where $\mathcal{H} = \dot{a}/a$ is the Hubble factor in conformal time, and for species $i$, $\delta_i = \delta\rho_i/\bar{\rho}$ is the fractional overdensity and $q_i$ is the heat flux and is related to the divergence of the peculiar velocity, $\theta_i$, by $\theta_i = \frac{k\ q_i}{1+w_i}$. Enforcing the conservation of energy-momentum on the perturbed matter fluid, these quantities for uncoupled fluid species or the mass-averaged quantities for all the fluids evolve as described in [67]:

$$\dot{\delta} = -kq + 3(1+w)\dot{\phi} + 3\mathcal{H}(w - c_s^2)\delta \tag{5}$$

$$\frac{\dot{q}}{k} = -\mathcal{H}(1-3w)\frac{q}{k} - \frac{\dot{w}}{1+w}\frac{q}{k} + c_s^2\delta - (1+w)\frac{\pi}{2} + (1+w)\psi. \tag{6}$$

Above, $w = p/\rho$ is the equation of state and $c_s^2 = \delta p/\delta\rho$ is the sound speed. Combining these two equations, we can express the evolution of $\Delta$ by:

$$\dot{\Delta} = 3(1+w)\dot{\phi} + 3\mathcal{H}w\Delta - \left[3\mathcal{H}\frac{\dot{w}}{1+w} + k^2 + 3\left(\mathcal{H}^2 - \dot{\mathcal{H}}\right)\right]\frac{q}{k} - 3\mathcal{H}(1+w)\left(\frac{\pi}{2} + \psi\right). \tag{7}$$

Equations (2),(3),(5), and (6) are coupled to one another, combining them, along with the evolution equations for $a(\tau)$, we can describe the growth history of structures in the universe.

### B. Modifications to the growth equations for detecting deviations from general relativity.

Recently, a lot of attention has gone into detecting deviations from general relativity by parameterizing both modifications to Poisson's equation, (2), as well as the ratio between the two metric potentials $\phi$ and $\psi$ in the perturbed FLRW metric (called *gravitational slip* by [11]), see for example [11, 53–57]. In this paper, we use two continuous parameterizations and a binned parameterization that allow for modifications of equations (2) and (3) both directly and indirectly.

### 1. Examples of parameterization with functional forms for time and scale dependencies

The first parameterization with a functional form that we use was proposed by [54]. It allows modifications to equations (2) and (3) that evolve monotonically in both time and scale, and makes no assumptions as to the time when a deviation from general relativity is allowed. These modifications are as follows:

$$k^2\phi \;=\; -4\pi G a^2 \sum_i \rho_i \Delta_i \, Q \tag{8}$$

$$k^2(\psi - R\,\phi) \;=\; -12\pi G a^2 \sum_i \rho_i (1+w_i)\frac{\pi_i}{2}\, Q, \tag{9}$$

where $Q$ and $R$ are the MG parameters. The parameter $Q$ represents a modification to the Poisson equation, while the parameter $R$ quantifies the gravitational slip (at late times, when anisotropic stress is negligible, $R = \psi/\phi$). These parameters are parameterized to evolve in time and scale as:

$$X(k,a) = \Big[X_0 e^{-k/k_c} + X_\infty(1 - e^{-k/k_c}) - 1\Big]\, a^s + 1, \tag{10}$$

where $X$ denotes either $Q$ or $R$. So the model parameters which can be used to detect deviations from GR are now: $Q_0$, $R_0$, $Q_\infty$, $R_\infty$, $k_c$, and $s$. The parameters $s$ and $k_c$ parameterize time and scale dependence respectively, with GR values $s = 0$ and $k_c = \infty$. $Q_0$ and $R_0$ are the present-day super-horizon values while $Q_\infty$ and $R_\infty$ are the present-day sub-horizon values of the $Q(k,a)$ and $R(k,a)$ , all taking GR values of 1.

The second parameterization we use comes from [57] and is used in their code `MGCAMB` [68]. Here, a modification to equation (2) is done indirectly by defining a modified field equation containing the parameter $\mu$, as well as, a gravitational slip parameter, $\eta$. Explicitly these modifications are:

$$k^2\psi \;=\; -4\pi G a^2 \sum_i \rho_i \Delta_i \, \mu(k,a). \tag{11}$$

$$\frac{\phi}{\psi} \;=\; \eta(k,a) \tag{12}$$

The parameters, $\{\mu, \eta\}$ are allowed to have a redshift dependence where they are fit to constant values below some transition redshift, $z_s$, (note that this is not to be confused with the source galaxy distribution peak redshift) and then make a transition to a GR value of 1 as following a hyperbolic tangent function with a transition width, $\Delta z$:

$$\mu(z) \;=\; \frac{1-\mu_0}{2}\Big(1 + \tanh\frac{z - z_s}{\Delta z}\Big) + \mu_0, \tag{13}$$

$$\eta(z) \;=\; \frac{1-\eta_0}{2}\Big(1 + \tanh\frac{z - z_s}{\Delta z}\Big) + \eta_0. \tag{14}$$

Also, the parameterization uses one other parameter, $\Sigma(k,\, a)$, defined by:

$$\Sigma(k,a) \equiv -\frac{k^2(\psi+\phi)}{8\pi G\rho a^2 \Delta} = \frac{\mu(1+\eta)}{2} \tag{15}$$

but with only a redshift dependence here in this sub-section. As we discuss in sub-section C below, this parameter is useful to break degeneracies between the other parameters.

### 2. Example of parameterization with binning in time and scale

Thirdly, in order to allow for simultaneous scale (wavenumber) and redshift (time) dependences in the $(\mu(k,a), \Sigma(k,a))$ parameterization above, we use variants of a $2 \times 2$ binned approach (called pixellation in [57]). We use two bins for scale dependence as $0.0 < k \leq k_x$ and $k_x < k < \infty$, and where we use an analysis with $k_x = 0.01\, h\, Mpc^{-1}$ and the other with $k_x = 0.1\, h\, Mpc^{-1}$. In both cases, we bin for redshift dependence as $0 < z \leq 1$ and $1 < z \leq 2$. We also use a third redshift binning method with $0 < z \leq 1.5$ and $1.5 < z \leq 3$ and the scale bin separator at $k_x = 0.01\, h\, Mpc^{-1}$ for the datasets in this paper. We use combinations of the parameters $\mu_i$ and $\Sigma_i$ with $i = 1...4$ for each $[k,\, z]$ bins in a $2 \times 2$ grid as shown in Table I. Transitions between the redshift bins behave as a hyperbolic tangent function with a transition width of $\Delta z = 0.05$ (almost a step), while transitions between scale bins are straightforward steps.

| | Redshift bins | |
|---|---|---|
| Scale bins | $0.0 < z \leq 1$, 1.5 | 1, $1.5 < z \leq 2$, 3 |
| $0.0 < k \leq k_x$ | $\mu_1$, $\Sigma_1$ | $\mu_2$, $\Sigma_2$ |
| $k_x < k < \infty$ | $\mu_3$, $\Sigma_3$ | $\mu_4$, $\Sigma_4$ |

TABLE I: The layout of the binned parameterizations. Specifically, for the first two binned methods this involves using $\{\mu_1, \Sigma_1\}$ for the $0 < z \leq 1$ and $0.0 < k \leq k_x$ bin, $\{\mu_2, \Sigma_2\}$ for the $1 < z \leq 2$ and $0.0 < k \leq k_x$ bin, $\{\mu_3, \Sigma_3\}$ for the $0 < z \leq 1$ and $k_x < k < \infty$ bin, and $\{\mu_4, \Sigma_4\}$ for the $1 < z \leq 2$ and $k_x < k < \infty$ bin, and the third binned method uses $\{\mu_1, \Sigma_1\}$ for the $0 < z \leq 1.5$ and $0.0 < k \leq k_x$ bin, $\{\mu_2, \Sigma_2\}$ for the $1.5 < z \leq 3$ and $0.0 < k \leq k_x$ bin, $\{\mu_3, \Sigma_3\}$ for the $0 < z \leq 1.5$ and $k_x < k < \infty$ bin, and $\{\mu_4, \Sigma_4\}$ for the $1.5 < z \leq 3$ and $k_x < k < \infty$ bin.

### C. Relations between parameterizations and degeneracies among parameters

We now turn our discussion to relating the different parameterizations to one another. We will focus on the $\{Q, R\}$ and $\{\mu, \eta, \Sigma\}$ parameterizations above, as well as, a third parameterization using $\{\mathcal{G}, \mathcal{V}\}$ used in[56]. When relating the `MGCAMB` and $\{\mathcal{G}, \mathcal{V}\}$ parameterizations to that of the first, we give the relations during matter domination, assuming zero anisotropic stress.

$$\mu = QR = \mathcal{V} \qquad , \qquad \eta = \frac{1}{R} = 2\frac{\mathcal{G}}{\mathcal{V}} - 1 \tag{16}$$

$$\Sigma = \frac{Q(1+R)}{2} = \mathcal{G} \qquad , \qquad \mu\eta = Q = 2\mathcal{G} - \mathcal{V}. \tag{17}$$

We use these relations later in order to infer constraints on some parameters from the ones obtained from the constrained derived from the datasets.

As previously pointed out [54–57] some of these parameters are degenerate and it is worth introducing parameters that alleviate these degeneracies. First, the parameters $Q_{0,\infty}$ and $R_{0,\infty}$ are degenerate along a direction that we call $D_{0,\infty} = Q_{0,\infty}(1 + R_{0,\infty})/2$ this degeneracy is shown with a curve in Figure 1. We proceed by varying $Q_{0,\infty}$ and $D_{0,\infty}$ and infer values of $R_{0,\infty}$ from the two parameters. Similarly, $\mu$ and $\eta$ are degenerate along curves of $\Sigma =$ constant so we vary $\mu$ and $\Sigma$ to get rid of this degeneracy. Using the parameters $D$ and $\Sigma$ is also useful because observations of the weak lensing and ISW are sensitive to the sum of the metric potentials $\phi + \psi$ and its time derivative respectively. Thus observations are able to give us direct measurements of these parameters.

### D. Figures of merit

We calculate the figures of merit (FoM) for the parameter pairs used for each parameterization considered. The FoM approach has been used previously, for example, to quantify the constraining power of cosmological data on the dark energy equation of state parameters, using simulated future data [41, 69–73], or current data [74–76]. For a pair of parameters, the FoM can be defined to be proportional to the inverse of the 95% confidence limit area. For more parameters, this can be generalized to be proportional to the inverse of the volumes and super-volumes of the (super-) ellipsoids, again representing the confidence limits in these parameter hyperspaces. A variety of choices for the constants of proportionality has been made in previous work and we simply chose to set it to one. Assuming a Gaussian distribution, the FoM for two parameters is inversely proportional to the area of the ellipse comprising the contour of constraints for the two parameters and so we define our FoM [74],

$$\text{FoM} = (det\, C)^{-1/2} \tag{18}$$

where $C$ is the 2D covariance matrix for the two parameters [77]. This is similar to the FoM used by the Dark Energy Task Force for the equations of state parameters. Obviously, tighter constraints lead to higher FoMs.

For two uncorrelated parameters with Gaussian uncertainties, the FoM doesn't provide any more information than the individual uncertainties in describing the constraining power of the datasets [69], but our results are not purely gaussian, and our parameters that we show FoM's for are not always uncorrelated. The FoM's are very informative to tell us which dataset is most significant in constraining the parameters and in our study here, was useful in indicating some tension between the datasets. It is of course understood that the FoM as we have defined it here, is only an approximation with non-Gaussian uncorrelated parameters, but accurate within $\sim 10\%$ in the worst cases [74]. The FoM is less accurate for two degenerate parameters, but still provides a good approximation to compare the constraining power of datasets. In fact, at first glance, when looking at the constraints in the tables and figures below,

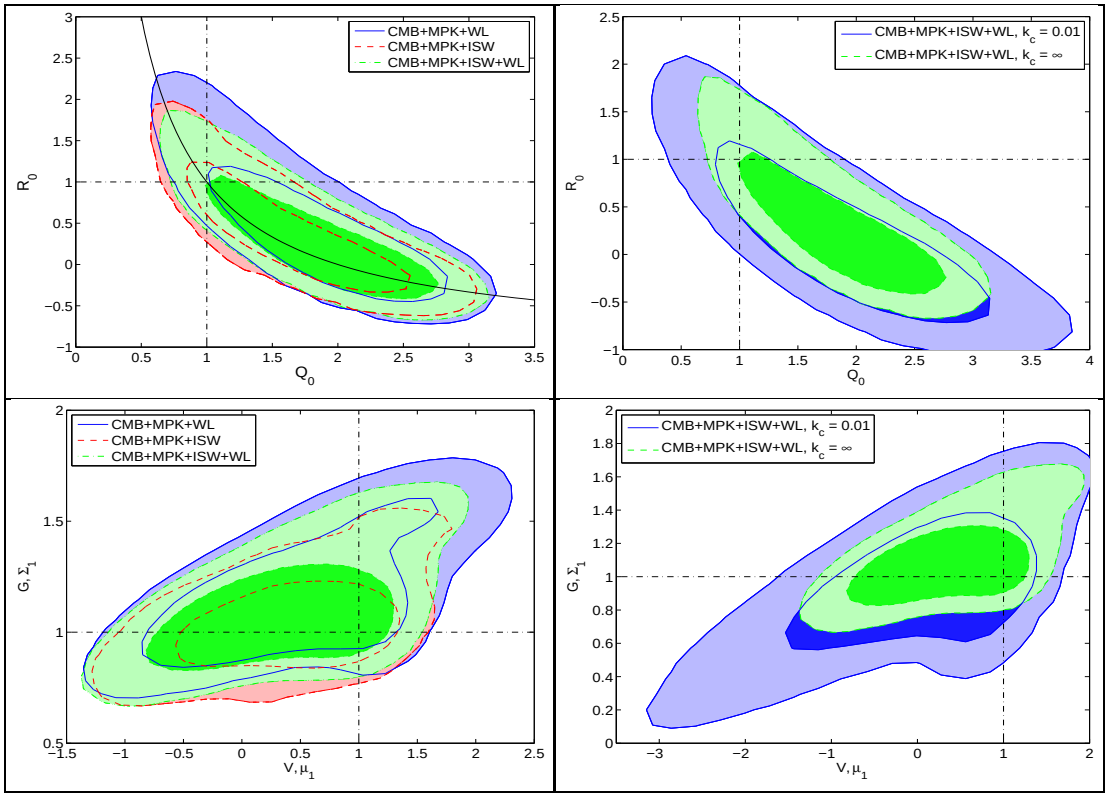


FIG. 1: TOP: 68% and 95% C.L. for the constraints on $Q_0$ and $R_0$. TOP-LEFT: Constraints with $Q$ and $R$ scale-independent ($k_c = \infty$). To show how the parameter $D_0$ actually represents the degeneracy direction of these parameters, the solid black line is the line $D_0 = 1$. TOP-RIGHT: A comparison of constraints when $Q$ and $R$ are allowed either scale-dependence ($k_c = 0.01$) or scale-independence using CMB, ISW, MPK, and WL. Scale-dependent constraints are in red and scale-independent constraints in blue. BOTTOM-LEFT: Inferred 68% and 95% C.L. constraints for the parameters $\mathcal{G}$ or $\Sigma_1$ and $\mathcal{V}$ or $\mu_1$ in the second and third parameterizations [56, 57]. These constraints are inferred by using constraints on the parameters $Q_0$, $R_0$, and $D_0$ from the first parameterization [54]. For all of these constraints we set $k_c = \infty$ implying scale independence of the parameterization (10). BOTTOM-RIGHT: We compare inferred constraints on $\mathcal{G}$ or $\Sigma_1$ and $\mathcal{V}$ or $\mu_1$ using CMB, ISW, MPK, and WL when scale-dependence is allowed in the first parameterization to constraints when the parameterization is scale-independent.

without the FoM, it is more difficult to determine which combination of datasets is more sensitive because at times there is a shift in the allowed parameter space for the different combinations of datasets.

This metric is useful in order to compare the constraining power of various combinations of the datasets that we used, namely WMAP7 temperature and polarization spectrum (CMB), the matter power spectrum (MPK), ISW-galaxy cross correlations (ISW) and HST COSMOS weak lensing tomography (WL). In each case, we use Union2 supernovae (SN), BAO, BBN, Age and $H_0$, as well.

## III. DATASETS FOR OBSERVATIONAL CONSTRAINTS

We use Type Ia SNe from the Union2 compilation[63], BAO from 2dF and SDSS DR7 [60, 61], and WMAP7 spectrum. The WMAP7 data, MPK from SDSS DR7 [60], the ISW-galaxy cross correlations [64, 65] and COSMOS weak lensing tomography [66] will constrain the growth as described below. We compare to the full temperature (TT) and polarization (TE) spectra using the WMAP 7-year data release using the likelihood routine provided by the WMAP team [62]. Next, for the BAO, we follow the most recent comparison [60, 61] and define the ratio of the sound horizon, $r_s(z_d)$ to the effective distance, $D_V$ as a fit for SDSS. We also add the prior $H_0 = 74.2 \pm 3.6$ km/s/Mpc given by [78], and the priors on the age of the Universe (AGE) 10 Gyrs$<$AGE$<$ 20 Gyrs, and $\Omega_b h^2 = 0.022 \pm 0.002$ from Big Bang Nucleosynthesis (BBN) . A possible deviation from GR is allowed by the modified Poisson equation and inequality between $\phi$ and $\psi$. The growth of structure is important in constraining the model parameters for a deviation from GR in this modified description. For the total matter power spectrum today, for example, see [54], we

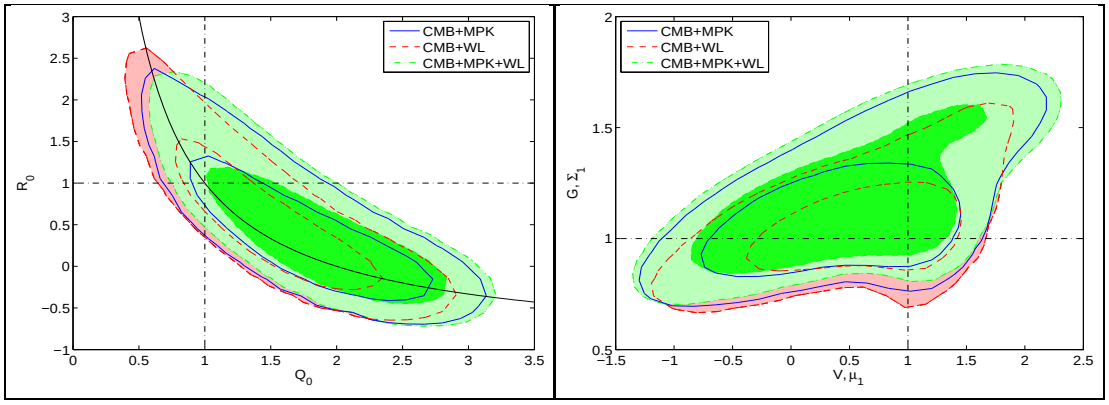


FIG. 2: We compare the 68% and 95% C.L. constraints on the $Q_0$ and $R_0$ (LEFT) as well as the inferred parameters $\mathcal{G}$ or $\Sigma_1$ and $\mathcal{V}$ or $\mu_1$ (RIGHT) for CMB+MPK (blue) and CMB+WL (red) and CMB+MPK+WL (green) to show the tension between these datasets. Notice the combined constraints are outside those of the individual datasets.

use

$$P(k) = 2\pi^2 \Big(\frac{k}{h}\Big)^3 \Delta^2_{tot}, \tag{19}$$

where $\Delta_{tot} = (\rho_c \Delta_c + \rho_b \Delta_b)/(\rho_c + \rho_b)$ is the gauge invariant, rest frame, over-density for CDM and baryons combined. Recall, that the matter power spectrum is sensitive to the growth of structure by constraining $\mu$ through $\Delta$ [54, 56, 57]. WMAP7 data also provides large scale ISW measurements. The ISW effect describes the evolution in time of the gravitational potentials. The photons from the CMB gain energy falling into varying potential wells, and may not return it all on exit. This causes a secondary anisotropy of the CMB and can be analyzed directly with the derivatives of $\phi$ and $\psi$ to give an indication of deviation from GR, as described in [54, 56, 57]. It is difficult to distinguish these CMB temperature anisotropies signatures from rest of CMB anisotropies because it has 1/10 the amplitude, so we need to correlate this effect to the large scale structure (LSS) of the universe. For this we use the ISW-galaxy cross-correlations which includes the use of 2MASS and SDSS LRG galaxy auto-correlations explored in [64, 65] and recently used by [54, 56].

We further constrain the parameters with expansion history and the effect of the growth of structure from the weak lensing tomography shear-shear cross-correlations of the HST COSMOS survey recently compiled by Schrabback et. al. [66]. The weak lensing constrains the growth of structure through the combination of $\phi$ and $\psi$ as described in [54, 56, 57]. The authors of [66] perform a refined analysis of the HST COSMOS survey of [79], in combination with the COSMOS-30 photometric redshift catalogue provided by [80]. The shear-shear cross-correlations were calculated between 6 redshift bins, $0.0 < z < 0.6$, $0.6 < z < 1.0$, $1.0 < z < 1.3$, $1.3 < z < 2.0$, $2.0 < z < 4.0$ and a sixth bin that contains all faint galaxies with a numerically estimated redshift distribution from $0.0 < z < 5.0$, see Figure 6 of [66]. Certain exclusions were made as described in [66], such as the LRGs to avoid G-I intrinsic alignment bias and the lowest angular theta bin because of model uncertainties. Only bright galaxies ($i < 24$) were used in the first bin ($z < 0.6$). Also, auto-correlations were not used in bins $1 - 5$ to reduce the effect of I-I intrinsic alignments. For comparing the shear-shear cross-correlations, we modify the publically available code for the COSMOS 3D weak lensing built by Lesgourgues et. al. [81] to incorporate the shear cross-correlations as seen in, for example, [66] (see footnote [89]).

For the ISW-galaxy cross correlations we modified our code as described in previous works [54, 56, 57] and refer the readers to those works for an extended discussion of the implications of these modifications. Here, however, we use the newly refined HST-COSMOS 3D weak lensing tomography by [66] and describe the modeling of this data below (We note that during the preparation of this manuscript, [59] released a paper fitting MG parameters using this dataset as well).

In order to model the weak lensing, the shear cross-correlation functions $\xi^{kl}_{+,-}(\theta)$ between bins $k, l$ are given by:

$$\xi^{kl}_{+,-}(\theta) = \frac{1}{2\pi} \int_0^\infty d\ell \; \ell \; J_{0,4}(\ell\theta) P^{kl}_\kappa(\ell), \tag{20}$$

where $J_n$ is the $n^{th}$-order Bessel function of the first kind, $\ell$ is the modulus of the two-dimensional wave vector, and $P^{kl}_\kappa$ is the convergence cross-power spectra between bins $k, l$. These cross-power spectra are computed from integrating

the three-dimensional (non-linear) power spectrum $P_\delta$,

$$P_\kappa^{kl}(\ell) = \frac{9H_0^4\Omega_m^2}{4c^4}\int_0^{\chi_h} d\chi \frac{g_k(\chi)g_l(\chi)}{a^2(\chi)} P_\delta\Big(\frac{\ell}{f_K(\chi)}, \chi\Big), \tag{21}$$

with comoving radial distance $\chi$, comoving distance to the horizon $\chi_h$, and comoving angular diameter distance $f_K(\chi)$. We note here that the effect of the MG parameters on the input power spectrum from the transfer function has been implemented in our weak lensing code, while the effect of the growth has been accounted for by our modifications to `CAMB` [82], and both are included in $P_\delta$ of equation (21). Also, following [66], we weight the geometric lens-efficiency factors

$$g_k(\chi) \equiv \int_\chi^{\chi_h} d\chi' p_k(\chi') \frac{f_K(\chi'-\chi)}{f_K(\chi')}, \tag{22}$$

corresponding to the redshift distributions $p_k$ for the two compared redshift bins. We use the $160 \times 160$ dimensional covariance matrix provided by Schrabback et. al. [66] and for the corresponding weak shear correlations. We also apply the correction to the inverse covariance, $Cov^{-1}$, seen in [66, 84], as

$$\overset{*}{Cov}{}^{-1} = 0.4390\, Cov^{-1}. \tag{23}$$

for 288 independent realizations and a 160 dimensional data vector. Following instruction from [66], we weight the predictions for the $k^{th}$ $\theta$ bin, $\theta_k$, with logarithmic spaced upper and lower limits $\theta_{k,max}$ and $\theta_{k,min}$, respectively, based on the number of galaxy pairs,$N$ for a given $\theta$ as

$$\xi(\theta_k) = \frac{\int_{\theta_{k,min}}^{\theta_{k,max}} N(\theta')\xi_{+,-}(\theta')d\theta'}{\int_{\theta_{k,min}}^{\theta_{k,max}} N(\theta')d\theta'}, \tag{24}$$

with $N(\theta) \propto \theta(0.0004664 + \theta(0.0044118 - 8.90878 \times 10^{-5}\theta))$ where the units of $\theta$ is arcminutes. [66, 85]. Finally, the 10% uncertainty in the numerical estimate of the galaxy redshift distribution of bin 6 is applied, following [66], as $p_6(z, f_z) \equiv p_6(f_z z)$, where $f_z$ is a nuissance parameter marginalized in the results below.

## IV. RESULTS AND DISCUSSION

Monte Carlo Markov Chains (MCMC's) are used to compute the likelihoods for the parameters in the model. This method randomly chooses values for the above parameters and, based on the $\chi^2$ obtained, either accepts or rejects the set of parameters via the Metropolis-Hastings algorithm. When a set of parameters is accepted it is added to the chain and forms a new starting point for the next step. The process is repeated until the specified convergence is reached (via Raftery-Lewis convergence criterion). We perform the best fit of the parameters in the various models by $\chi^2$ minimization, i.e. minimizing for example $\chi^2 = \chi^2_{SN} + \chi^2_{BAO} + \chi^2_{CMB} + \chi^2_{ISW} + \chi^2_{WL} + \chi^2_{MPK}$ via a maximum likelihood analysis. To get best fits for the MG parameters of a given parameterization we use, as discussed above modified versions of the publicly available ISW and Weak Lensing Likelihood code [64], HST-COSMOS weak lensing code [81], `CAMB` [82], and `CosmoMC` [83]. For these modified codes, see [89]. We fix the dark energy equaiton of state $w = -1$ assuming a $\Lambda$CDM expansion. Then in addition to varying the MG parameters for a given parameterization, we vary the six core cosmological parameters: $\Omega_b h^2$ and the $\Omega_c h^2$, the baryon and cold-dark matter physical density parameters, respectively; $\theta$, the ratio of the sound horizon to the angular diameter distance of the surface of last scattering; $\tau_{rei}$, the reionization optical depth; $n_s$, the spectral index; and $\ln 10^{10} A_s$, the amplitude of the primordial power spectrum. These parameters are allowed to vary within the wide range of values that are defaulted in the `params.ini` file of `CosmoMC`. Additionally, as discussed in the previous section, when using the WL dataset we marginalize over the nuissance parameter $f_z$. We provide various 95% confidence limits on the MG parameters along with the corresponding contour plots. We also calculate the figure of merit (FoM) for the parameter combinations for the parameterization considered.

As described above,for the first parameterization, i.e. equations (8) and (9), we follow the technique of varying $Q_{0,\infty}$ and $D_{0,\infty} = Q_{0,\infty}\,(1 + R_{0,\infty})\,/2$, while inferring values of $R_{0,\infty}$ from the other two parameters. We allow these

| **Constraints for the parameters** $\{Q_{0,\infty}, R_{0,\infty}, D_{0,\infty}\}$ | | | | | | | | |
|---|---|---|---|---|---|---|---|---|
| $k_c = \infty$ | | | | | | | | |
| Dataset | $\mathrm{FOM}_{Q_0;R_0}$ | $\mathrm{FOM}_{Q_0;D_0}$ | $Q_0$ | $R_0$ (derived) | $D_0$ | $Q_\infty$ | $R_\infty$ (derived) | $D_\infty$ |
| CMB, MPK | 5.53 | 8.81 | [0.69, 2.79] | [−0.34, 2.04] | [0.79, 1.62] | – | – | – |
| CMB, ISW | 6.15 | 9.80 | [0.70, 2.76] | [−0.33, 1.85] | [0.79, 1.55] | – | – | – |
| CMB, WL | 6.44 | 12.15 | [0.57, 2.54] | [−0.30, 2.24] | [0.76, 1.47] | – | – | – |
| CMB, ISW, WL | 8.46 | 14.96 | [0.67, 2.53] | [−0.33, 1.84] | [0.75, 1.34] | – | – | – |
| CMB, MPK, ISW | 7.53 | 11.97 | [0.80, 2.73] | [−0.35, 1.62] | [0.76, 1.46] | – | – | – |
| CMB, MPK, WL | 5.08 | 7.96 | [0.73, 2.80] | [−0.34, 2.13] | [0.82, 1.65] | – | – | – |
| CMB, MPK, ISW, WL | 7.09 | 10.06 | [0.83, 2.82] | [−0.37, 1.60] | [0.77, 1.56] | – | – | – |
| $k_c = 0.01$ | | | | | | | | |
| Dataset | $\mathrm{FOM}_{Q_0;R_0}$ | $\mathrm{FOM}_{Q_0;D_0}$ | $Q_0$ | $R_0$ (derived) | $D_0$ | $Q_\infty$ | $R_\infty$ (derived) | $D_\infty$ |
| CMB, MPK, ISW, WL | 4.07 | 4.53 | [0.57, 3.35] | [−0.79, 1.67] | [0.29, 1.60] | [0.46, 4.01] | [−0.82, 2.28] | [0.26, 2.00] |

| **Inferred parameter constraints on the parameters** $\mathcal{G}$, $\Sigma_1$ **and** $\mathcal{V}$, $\mu_1$ **from parameters** $Q_0$, $R_0$, **and** $D_0$ | | | |
|---|---|---|---|
| $k_c = \infty$ | | | |
| Dataset | $\mathrm{FOM}_{\mathcal{G};\mathcal{V}}$ | $\mathcal{G}$,$\Sigma_1$ | $\mathcal{V}$,$\mu_1$ |
| CMB, MPK | 8.81 | [0.79, 1.62] | [−0.90, 1.79] |
| CMB, ISW | 9.80 | [0.79, 1.55] | [−0.86, 1.57] |
| CMB, WL | 12.15 | [0.76, 1.47] | [−0.72, 1.60] |
| CMB, ISW, WL | 14.95 | [0.75, 1.34] | [−0.78, 1.38] |
| CMB, MPK, ISW | 11.97 | [0.76, 1.46] | [−0.89, 1.42] |
| CMB, MPK, WL | 7.96 | [0.82, 1.65] | [−0.90, 1.91] |
| CMB, MPK, ISW, WL | 10.06 | [0.77, 1.56] | [−0.98, 1.57] |
| $k_c = 0.01$ | | | |
| Dataset | $\mathrm{FOM}_{\mathcal{G};\mathcal{V}}$ | $\mathcal{G}$,$\Sigma_1$ | $\mathcal{V}$,$\mu_1$ |
| CMB, MPK, ISW, WL | 4.53 | [0.29, 1.60] | [−2.46, 1.48] |

TABLE II: TOP: 95% C.L. for the parameters $Q_0$, $R_0$,$D_0$, $Q_\infty$, $R_\infty$, and $D_\infty$ in the first parameterization [54]. For these constraints, we marginalize over the parameter $s$ which characterizes the redshift (time) dependence of the parameterization. BOTTOM: Inferred 95% C.L. constraints for the parameters $\mathcal{G}$ or $\Sigma_1$ and $\mathcal{V}$ or $\mu_1$ in the second and third parameterizations [56, 57]. These constraints are inferred by using constraints on the parameters $Q_0$, $R_0$, and $D_0$ from the first parameterization [54].

parameters to vary $0 < Q_{0,\infty} < 10$, $0 < D_{0,\infty} < 10$, additionally ruling out parameter combinations where $R_{0,\infty} < -1$. We fit both scale independent and scale dependent forms of this parameterization, in both cases we allow for time dependence by marginalizing over the parameter $s$ as described earlier. For scale independent modifications, we fix $k_c = \infty$ and of course vary only the parameters $Q_0$ and $D_0$, while for scale dependent modifications we fix $k_c = 0.01$, allowing all four parameters $Q_{0,\infty}$ and $D_{0,\infty}$ to vary. The 95% CL's on these parameters and corresponding FoM's for various combinations of cosmological probes are given in Table II. We also plot the 68% and 95% 2D contours for $Q_0$ and $R_0$ in Figure 1. We find in all cases consistency with General Relativity at the 95% confidence level.

We note here that we don't find the slight $2\sigma$ deviation from GR on the parameter $Q_0$ seen in [54] when combining all the datasets. Rather in all cases for this parameterization we find parameter values consistent with General Relativity at the 95% confidence level and a little looser than the results given in [54]. We were however able to reproduce almost exactly the same results of [54] but only when fixing the core cosmological parameters to their WMAP7 [62] best fit values and allowing only the MG parameters to vary. We believe that the method of varying all the cosmological parameters simultaneously with the MG parameters gives more realistic and conservative results and those are the results that we reported in our Table II and Figures 1 and 2

Next, using the constraints we attained on the parameters of the first parameterization [54] we can, with the help of equations (16) and (17), infer constraints on the low redshift large scale parameters ($\mu_1$ and $\Sigma_1$ below) and ($\mathcal{G}$ and $\mathcal{V}$ in the low redshift and small $k-$ bin therein). We list these inferred 95% CL's and their FoM's in the second part of Table II and plot the 68% and 95% 2D contours in Figure 1. We verified that the shapes of the contours plotted for the inferred parameters reflect the physical priors placed on the non-inferred parameters as discussed above. Again, these results show consistency with General Relativity at the 95% confidence level.

Using the first parameterization, we find that the combination CMB+ISW+WL provides the strongest constraints on the parameters. We also observed that there seems some tension between current WL and MPK data. This reveals itself particularly well when comparing the FoM's of fits that include both these datasets to those that include only

| **Constraints on $\mu_0$, $\eta_0$, and $\Sigma_0$ for redshift dependence** | | | | | | | | |
|---|---|---|---|---|---|---|---|---|
| | $z_s = 1$ | | | | $z_s = 2$ | | | |
| $\Delta z = 0.05$ | | | | | | | | |
| Dataset | FoM | $\mu_0$ | $\Sigma_0$ | $\eta_0$ (derived) | FoM | $\mu_0$ | $\Sigma_0$ | $\eta_0$ (derived) |
| CMB, WL | 94.61 | [0.621, 1.622] | [0.948, 1.100] | [0.233, 2.328] | 162.5 | [0.645, 1.351] | [0.946, 1.080] | [0.467, 2.206] |
| CMB, MPK | 100.9 | [0.618, 1.557] | [0.955, 1.103] | [0.297, 2.350] | 177.0 | [0.618, 1.298] | [0.955, 1.079] | [0.542, 2.327] |
| CMB, ISW | 114.2 | [0.590, 1.427] | [0.954, 1.105] | [0.415, 2.505] | 196.0 | [0.635, 1.228] | [0.952, 1.082] | [0.637, 2.251] |
| CMB, MPK, WL | 104.5 | [0.624, 1.549] | [0.960, 1.108] | [0.317, 2.334] | 179.4 | [0.643, 1.331] | [0.959, 1.082] | [0.514, 2.221] |
| CMB, ISW, WL | 123.9 | [0.589, 1.399] | [0.954, 1.098] | [0.438, 2.499] | 209.2 | [0.627, 1.198] | [0.954, 1.081] | [0.658, 2.297] |
| CMB, MPK, ISW | 132.9 | [0.594, 1.355] | [0.956, 1.098] | [0.487, 2.472] | 230.2 | [0.608, 1.157] | [0.957, 1.076] | [0.723, 2.372] |
| CMB, MPK, ISW, WL | 132.5 | [0.592, 1.345] | [0.961, 1.106] | [0.520, 2.483] | 229.1 | [0.626, 1.182] | [0.962, 1.081] | [0.706, 2.307] |
| Marginalizing over $\Delta z$ | | | | | | | | |
| Dataset | FoM | $\mu_0$ | $\Sigma_0$ | $\eta_0$ (derived) | FoM | $\mu_0$ | $\Sigma_0$ | $\eta_0$ (derived) |
| CMB, MPK, ISW, WL | 74.29 | [0.618, 1.371] | [0.963, 1.226] | [0.527, 2.471] | 194.0 | [0.674, 1.176] | [0.957, 1.113] | [0.706, 2.089] |
| | $z_s = 3$ | | | | $z_s = 0.76$ | | | |
| $\Delta z = 0.05$ | | | | | | | | |
| Dataset | FoM | $\mu_0$ | $\Sigma_0$ | $\eta_0$ | FoM | $\mu_0$ | $\Sigma_0$ | $\eta_0$ |
| CMB, WL | 223.9 | [0.709, 1.249] | [0.944, 1.075] | [0.578, 1.906] | 75.74 | [0.631, 1.676] | [0.944, 1.119] | [0.209, 2.276] |
| CMB, MPK | 231.4 | [0.678, 1.214] | [0.955, 1.076] | [0.637, 2.063] | 83.27 | [0.629, 1.622] | [0.952, 1.122] | [0.254, 2.281] |
| CMB, ISW | 250.9 | [0.724, 1.179] | [0.949, 1.082] | [0.684, 1.861] | 89.01 | [0.606, 1.531] | [0.949, 1.121] | [0.331, 2.410] |
| CMB, MPK, WL | 225.8 | [0.709, 1.246] | [0.952, 1.077] | [0.602, 1.911] | 83.35 | [0.629, 1.625] | [0.955, 1.124] | [0.258, 2.302] |
| CMB, ISW, WL | 288.1 | [0.717, 1.146] | [0.951, 1.076] | [0.721, 1.881] | 87.78 | [0.599, 1.539] | [0.944, 1.115] | [0.313, 2.424] |
| CMB, MPK, ISW | 296.6 | [0.681, 1.109] | [0.954, 1.077] | [0.797, 2.045] | 96.48 | [0.600, 1.488] | [0.948, 1.115] | [0.358, 2.428] |
| CMB, MPK, ISW, WL | 316.9 | [0.703, 1.127] | [0.961, 1.076] | [0.769, 1.961] | 95.59 | [0.603, 1.492] | [0.955, 1.121] | [0.368, 2.423] |
| Marginalizing over $\Delta z$ | | | | | | | | |
| Dataset | FoM | $\mu_0$ | $\Sigma_0$ | $\eta_0$ | FoM | $\mu_0$ | $\Sigma_0$ | $\eta_0$ |
| CMB, MPK, ISW, WL | 272.8 | [0.729, 1.139] | [0.956, 1.095] | [0.758, 1.859] | 43.15 | [0.589, 1.559] | [0.948, 1.298] | [0.361, 2.689] |

TABLE III: The FoM for each dataset and $\{\mu_0, \Sigma_0\}$ is given.95% C.L. for the parameters $\mu_0$, $\eta_0$, and $\Sigma_0$ from the second parameterization [57, 68] for redshift dependence $z_s = 1$, 2, 3 for different combinations of datasets. We also add the physically motivated transition redshift (from deceleration to acceleration in an LCDM model) given by $1 + z_{trans} = (2\Omega_\Lambda/\Omega_m)^{1/3} \approx 1.76$ (for example see equation (14) in [86]) for comparison. The data used is described in the text above and indicated as: WMAP7 temperature and polarization spectrum (CMB), the matter power spectrum (MPK), ISW-galaxy cross correlations (ISW), weak lensing tomography (WL). In all cases, the data used is combined with SN, BAO, BBN, AGE and $H_0$.

one of them eg. CMB+MPK+WL vs CMB+WL. Similarly, the combinations CMB+ISW+WL or CMB+MPK+ISW does better than the combination CMB+MPK+ISW+WL. In order to investigate this, we compared the best fit models preferred by each combination of datasets finding that significant tensions exist between the best fit values for the MG parameters when using this parameterization. There are no significant tensions between the core cosmological parameters. This tension is illustrated in Figure 2 for both constraints on $Q_0$ and $R_0$ as well as the inferred parameters $\mathcal{G}$ or $\Sigma_1$ and $\mathcal{V}$ or $\mu_1$. Also, in searching for the origin of this tension, we have both fixed the six core cosmological parameters to the WMAP7 values and additionally the time dependence parameter to $s = 3$, yet it persists, significantly. We also find that the second parameterization below does not exhibit this particular tension between WL and MPK but shows other tension although substantially less pronounced.

For the second parameterization, i.e. the one used in `MGCAMB` [57], we derive uncertainties and FoM for $\mu(k, a)$ and $\Sigma(k, a)$ to avoid the strong degeneracy between $\mu(k, a)$ and $\eta(k, a)$. In order to allow for the parameters to be redshift (time) dependent and scale (wavenumber) dependent, we use a binned approach to look for deviation from GR, with no functional form assumed for the parameters. First, however, we allow only redshift dependence in order to compare to the first parameterization [54] and look for deviation at late times, i.e. $z < z_s$ with a threshold redshift, $z_s = 0.76$, 1, 2, or 3 and assume that at early times $\mu(k, a) = \eta(k, a) = 1$. As a remainder, the evolution in time is described by (13) and (14). We use the transition width in (13) and (14) to be both fixed, $\Delta z = 0.05$, so that the transition is almost a step function, as well as, allowed to vary in the interval [0.01, 0.5], becoming a nuissance parameter marginalized over. We allow these parameters to vary as follows: $-10 < \mu_0 < 10$, $0 < \Sigma_0 < 10$, and ruling out parameter combinations where $\eta_0 < -1$. For each data set used, our results are given in Table III showing the FoMs and 95% confidence limits on $\mu_0$ and $\Sigma_0$, as well as the inferred constraints on $\eta_0$, for this case (i.e. redshift (time) dependence only). See Figure 3 for comparisons of the 95% confidence limit contours. We find that the general

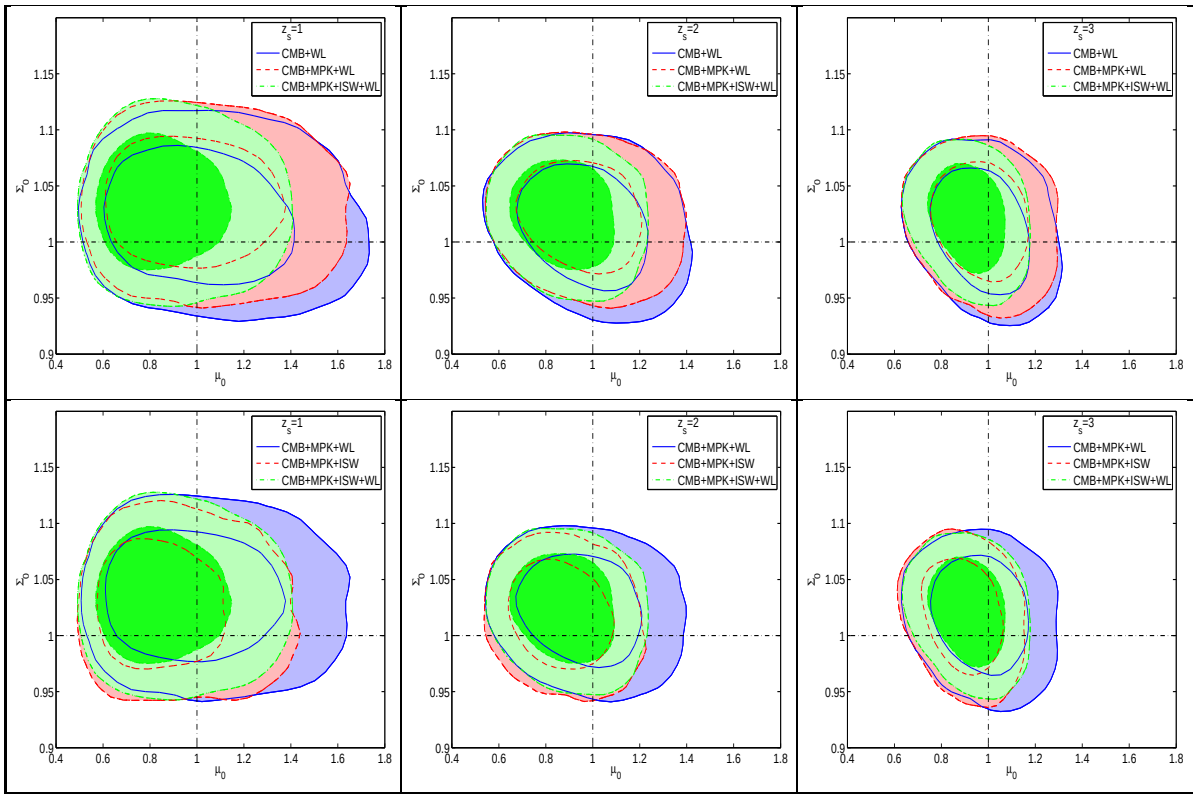


FIG. 3: TOP-LEFT:68% and 95% C.L. for the constraints on $\mu_0$ and $\Sigma_0$ of the second parameterization [57, 68] with threshold redshift, $z_s = 1$ and transition width fixed, $\Delta z = 0.05$. All contours are fit for CMB, SN, BAO, BBN, AGE and $H_0$. Blue (solid line) contours include WL, red (dashed line) contours include WL and MPK, and green (dashdot line) contours include WL, MPK, and ISW. TOP-CENTER: Same as LEFT, but for threshold redshift $z_s = 2$. TOP-RIGHT: Same as LEFT, but for threshold redshift $z_s = 3$. BOTTOM-LEFT:68% and 95% C.L. for the constraints on $\mu_0$ and $\Sigma_0$ of the second parameterization [57, 68] with threshold redshift, $z_s = 1$ and transition width fixed, $\Delta z = 0.05$. All contours are fit for CMB, MPK, SN, BAO, BBN, AGE and $H_0$. Blue (solid line) contours include WL, red (dashed line) contours include ISW, and green (dashdot line) contours include WL and ISW. BOTTOM-CENTER: Same as LEFT, but for threshold redshift $z_s = 2$. BOTTOM-RIGHT: Same as LEFT, but for threshold redshift $z_s = 3$. The point $(1, 1)$ indicates the GR values.

relativity values, ($\mu_0 = 1$, $\Sigma_0 = 1$), are within 95% confidence level for all datasets. The constraints from $z_s = 2$ are tighter than $z_s = 1$ because the earlier threshold redshift allows more change in gravitational potential and growth from the datasets, also noted in [57]. We also add constraints where we set the threshold redshift $z_s = 3$ taking advantage of the higher redshift (i.e. $2 < z \leq 3$) WL data in HST-COSMOS. We know that the relevant redshift for cosmic acceleration is much smaller, but it is of interest to simply study the constraints obtained on the growth of structure using various available ranges of data. From the physically motivated transition redshift (from deceleration to acceleration in an LCDM model) given by $1 + z_{trans} = (2\Omega_\Lambda/\Omega_m)^{1/3} \approx 1.76$ (for example, see equation (14) in [86] with $\Omega_\Lambda = 0.73$, $\Omega_m = 0.27$), we add $z_s = 0.76$ for comparison, also. The physically motivated transition redshift finds the weakest constraints and lowest FoM's due to less data below $z_s = 0.76$, but all results are consistent with GR.

The strongest constraints and highest FoM's we find come from using the combination CMB+MPK+ISW for both $z_s = 1$, 2, whereas, for $z_s = 3$ the tightest constraint comes from using all the datasets including lensing, i.e. CMB+MPK+ISW+WL because with $z_s = 3$, we allow more WL data below the threshold redshift to constrain the MG parameters which also yields a longer constant value at late times. We find that the FoM for CMB+ISW is better than the one for CMB+MPK, which in turn is better than the FoM for CMB+WL. This shows that the current ISW data provides indeed the strongest constraints on the MG parameters. Also, as shown on Table III, the allowance of the transition width, $\Delta z$, to vary (i.e. [0.01, 0.5]) loosens the constraints and reduced the FoM for all $z_s$ models. Now, as found for the first parameterization, here also, there is a slight decrease in the FoM and weakening of the constraints (for $z_s = 1$, 2) when WL is added to CMB+MPK+ISW, again, due to some tensions between the preferred MG parameters by different datasets. To investigate these tensions, here we also fixed the core cosmological parameters and left the MG parameters to vary. As a result, the FoM's increase consistently (but only moderately

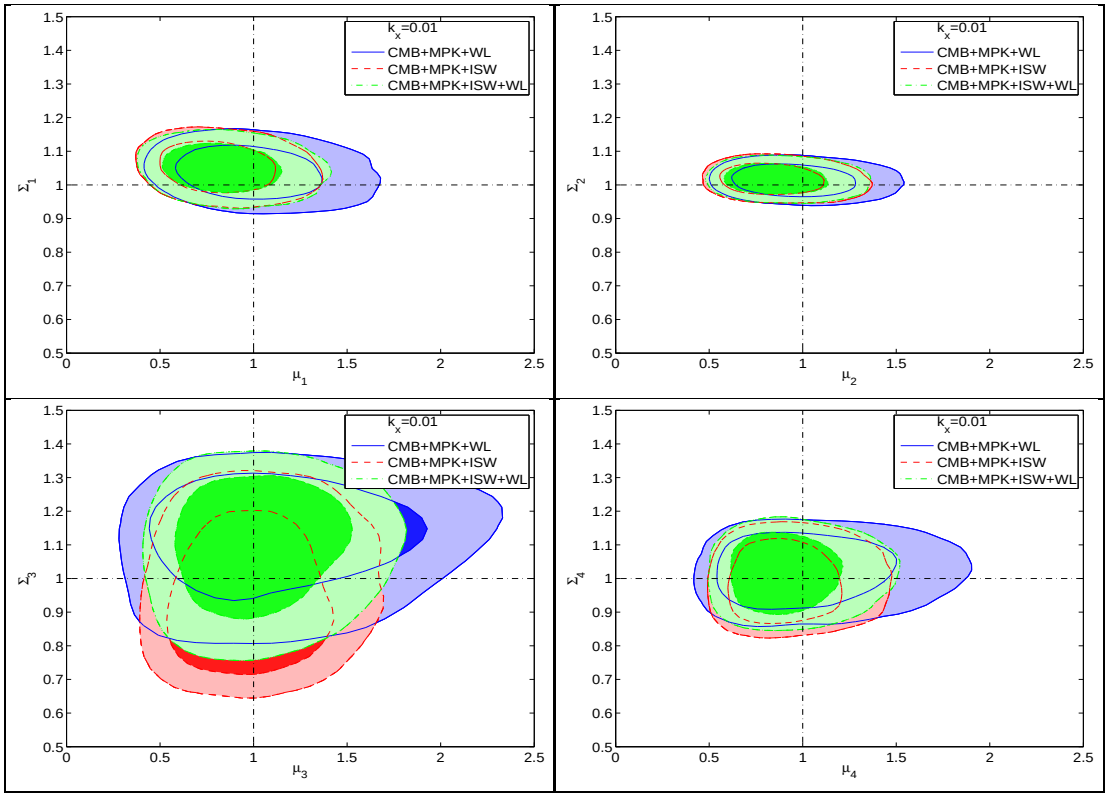


FIG. 4: 68% and 95% C.L. for the parameters $\mu_i$ and $\Sigma_i$ from the second parameterization [57, 68] for redshift and scale dependence as a binned $2 \times 2$ parameterization with $0 < z \leq 1$, $1 < z \leq 2$ and scale separation at $k_x = 0.01\,h\,Mpc^{-1}$. All contours are fit for CMB, MPK, SN, BAO, BBN, AGE and $H_0$. Blue (solid line) contours include WL, red (dashed line) contours include ISW, and green (dashdot line) contours include WL and ISW. The point $(1, 1)$ indicates the GR values.

in some cases) when adding a data set, indicating that some of the tension was reduced but not removed. In fact, a closer look at the best fit MG parameters preferred by different datasets shows that, while reduced, a non-negligible scatter is still present. This explains the only moderate improvements obtained in some cases. This indicates that there are non-negligible tensions intrinsic to the MG parameters preferred by different datasets.

Next, we calculate constraints and FoM's while we allow for simultaneous scale (wavenumber) and redshift (time) dependence by using variants of a $2 \times 2$ binned approach (called pixelization in [57]), see earlier discussion and Table I for details. We alternate between ISW and WL and their combination, while using CMB, MPK, BAO, SN, BBN, AGE and $H_0$ in all cases. We provide the FoM's and 95% confidence limits on $\mu_i$ and $\Sigma_i$, as well as, the inferred ones on $\eta_i$ in Table IV for scale dependence separators at $k_x = 0.01\,h\,Mpc^{-1}$ and $k_x = 0.1\,h\,Mpc^{-1}$, see Figures 4 and 5 for the comparisons in their C.L. contours. General relativity values for $\mu_i = 1$ and $\Sigma_i = 1$ are within all constraints for $\mu_i$ and $\Sigma_i$ for all the combination of datasets. Unlike the work that uses a binned parameterization and CFHTLS [56, 57], we do not find a deviation from GR with $\Sigma_3$. But as expressed there as well, this is due to the fact that we are using the refined HST COSMOS data by [66] which does not have the known systematic effect (i.e. residual systematic 'bump') as discussed in the papers using CFHTLS, [56, 57, 87, 88].

Another observation that can be made is that with the datasets used in this paper, the binning with scale separator at $k_x = 0.01\,h\,Mpc^{-1}$ better constrains $\{\mu_i, \Sigma_i\}$ by the balancing of the number of data points within the bins, so within each bin, we are taking maximum advantage of the available data. Whereas, the wave number separator at $k_x = 0.1\,h\,Mpc^{-1}$ does not equally balance the available data, i.e. $\{\mu_3, \Sigma_3\}$ and $\{\mu_4, \Sigma_4\}$ are not well constrained by ISW because most ISW data points are below $k_x = 0.1\,h\,Mpc^{-1}$, which allows WL to dominate the $\{\mu_3, \Sigma_3\}$ and $\{\mu_4, \Sigma_4\}$ bins. However, for bins with scale separator at $k_x = 0.01\,h\,Mpc^{-1}$, the FoM increases for $\{\mu_i, \Sigma_i\}$ in each bin beginning with the lowest for WL, then ISW, and the highest for the combination of ISW and WL because of the balance of data points, see Table IV, see Figure 4 (again CMB, MPK, BAO, SN, BBN, AGE and $H_0$ are included each time). There is a slight decrease of the FoM for the $\{\mu_1, \Sigma_1\}$ bin because there is not enough WL data in this

| **Constraints for $\{\mu_i, \Sigma_i\}$ binned parameterization $0 < z \leq 1$, $1 < z \leq 2$** | | | | | | |
|---|---|---|---|---|---|---|
| | $k_x = 0.01$ | | | $k_x = 0.1$ | | |
| Datasets | WL | ISW | ISW, WL | WL | ISW | ISW, WL |
| $\text{FoM}_1$ | 75.92 | 101.7 | 101.2 | 80.63 | 99.47 | 97.62 |
| $\mu_1$ | [0.559, 1.567] | [0.480, 1.227] | [0.494, 1.309] | [0.587, 1.540] | [0.542, 1.356] | [0.535, 1.357] |
| $\Sigma_1$ | [0.940, 1.138] | [0.957, 1.145] | [0.955, 1.139] | [0.946, 1.141] | [0.949, 1.136] | [0.951, 1.139] |
| $\eta_1$ (derived) | [0.281, 2.815] | [0.605, 3.486] | [0.563, 3.347] | [0.322, 2.644] | [0.493, 2.939] | [0.496, 3.004] |
| $\text{FoM}_2$ | 148.9 | 176.3 | 184.2 | 161.7 | 172.4 | 180.5 |
| $\mu_2$ | [0.614, 1.456] | [0.563, 1.289] | [0.580, 1.294] | [0.633, 1.413] | [0.635, 1.382] | [0.616, 1.335] |
| $\Sigma_2$ | [0.955, 1.072] | [0.959, 1.075] | [0.959, 1.072] | [0.955, 1.075] | [0.956, 1.072] | [0.957, 1.072] |
| $\eta_2$ (derived) | [0.376, 2.332] | [0.546, 2.649] | [0.554, 2.526] | [0.416, 2.238] | [0.452, 2.229] | [0.503, 2.329] |
| $\text{FoM}_3$ | 18.95 | 22.94 | 25.61 | 5.989 | 1.098 | 6.755 |
| $\mu_3$ | [0.439, 2.073] | [0.509, 1.588] | [0.544, 1.663] | [0.093, 2.771] | [0.122, 2.654] | [0.159, 2.519] |
| $\Sigma_3$ | [0.851, 1.321] | [0.708, 1.268] | [0.818, 1.319] | [0.903, 1.824] | [0.546, 5.391] | [0.871, 1.825] |
| $\eta_3$ (derived) | [0.069, 4.035] | [0.129, 2.889] | [0.244, 3.066] | [0.052, 26.31] | [0.051, 35.69] | [0.037, 14.78] |
| $\text{FoM}_4$ | 43.94 | 62.03 | 63.93 | 8.878 | 2.014 | 9.214 |
| $\mu_4$ | [0.553, 1.754] | [0.588, 1.404] | [0.593, 1.427] | [0.061, 1.269] | [0.032, 1.288] | [0.052, 1.194] |
| $\Sigma_4$ | [0.887, 1.148] | [0.858, 1.134] | [0.878, 1.144] | [0.173, 1.552] | [0.381, 5.181] | [0.167, 1.563] |
| $\eta_4$ (derived) | [0.152, 2.708] | [0.376, 2.424] | [0.398, 2.458] | [0.052, 18.46] | [0.024, 169.9] | [0.031, 22.27] |

TABLE IV: 95% C.L. for the parameters $\mu_i$, $\eta_i$, and $\Sigma_i$ from the second parameterization [57, 68] for redshift and scale dependence as a binned $2 \times 2$ parameterization with $0 < z \leq 1$, $1 < z \leq 2$ and scale separation at $k_x = 0.01\,h\,Mpc^{-1}$ and $k_x = 0.1\,h\,Mpc^{-1}$ . The data used is described in the text above and indicated as: ISW-galaxy cross correlations (ISW), weak lensing tomography (WL). In all cases, the data used is combined with WMAP7 temperature and polarization spectrum (CMB), the matter power spectrum (MPK), SN, BAO, BBN, AGE and $H_0$. The FoM for each dataset and $\{\mu_i, \Sigma_i\}$ bin is also given.

bin to increase the FoM when added to ISW. Some tension between ISW and WL datasets is more explicitly seen in bins $\{\mu_1, \Sigma_1\}$ and $\{\mu_2, \Sigma_2\}$ (see Table V) for both scale separators. Future surveys and other datasets may work better with scale separator at $k_x = 0.1\,h\,Mpc^{-1}$ [45].

We give the results for the third binned method in Table V and show the relevant ellipses for the FoM's in Figure 6. The constraints in Table V are tighter than the other binning results in table IV and have higher FoM's corresponding to smaller ellipses in Figure 6. The improvements in the constraints and FoM's comes from larger redshift bins allowing more data to constrain the parameters (called an *accumulation effect* by [57]) and these larger redshift bins also allowing a longer constant value for late times. The $\{\mu_2, \Sigma_2\}$ bin is slighter looser in this third binned method because more of the ISW data points are in the $\{\mu_1, \Sigma_1\}$ bin, now, due to a larger redshift bin, i.e. $0 < z \leq 1.5$, than in the previous two binned methods. We still observe some small tension when adding WL to the ISW dataset combination with the FoM's and contour plots, and it is more easily seen for example in the $\{\mu_1, \Sigma_1\}$ and $\{\mu_2, \Sigma_2\}$ bins in Table V where the FoM's rather decrease.

**Before to summarize our results further below it is worth discussing the possible physical origins of the tensions on best fit modified gravity parameters prefered by different combinations of datasets. To further explore this we decided to fix the core cosmological parameters to their WMAP7 values and use each set individually and removing CMB data-set since its data points will most likely dominate parameter constraints, and likley wash out some of the tension in our best fit parameter spaces. Our results expectedly gave us weak constraints and for both the first parameterization and the second parameterization (in its binned form), we continued to observe tensions where they had previously existed (the tension in the unbinned parameterization was removed by fixing the core cosmological parameters). The best fit parameter spaces obtained did give us further insight into the preferred parameter values of each data-set. For the first parameterization we saw that the best-fit for MPK preferred the lowest value of $s$ out of all the best fits. It additionaly, in contrast to WL best-fits, had negative best-fit values for $R$ and $\mathcal{V}$, though the best fit $Q$ and $D$ parameters are actually not that different between. Combining the two datasets however we find that a best fit for $s$ that is higher than either of the two datasets individually, additionally a higher $Q$ and correspondingly more negative $\mathcal{V}$ and $R$ are preferred. For the binned second parameterization we looked for tension between the MPK+ISW and WL dat-sets. In the first bin, the WL data-set had a much higher best-fit $\mu$ and $\Sigma$**

values than the MPK+ISW data-set. The MPK+ISW+WL dataset though has the lowest best fit $\Sigma_1$ and a similar besti-fit $\mu_1$ to the MPK+ISW dataset again showing the tension when combining these data-sets. These markedly different best fit values in the modified gravity parameter space between the individual and combined data-sets highlight the tension but do not explain it.

Working again with the first parameterization to explore the tension there, we next looked at the ouptut matter power spectrum for each of the best-fit parameter sets. This showed just how much an exacerbation the parameter $s$ may be causing. The amplitude of the matter power spectrum produced with the best-fit WL parameter set was two orders of magnitude greater than the amplitude of the spectrum produced by the best-fit MPK parameter set. Upon seeing this marked difference in amplitudes one can recall that in calculating the likelihood for MPK the amplitude of the power-spectrum is treated as a nuissance parameter [60]. This may be one reason for the tension when combining data-sets, as a number of MG parameter combinations can produce matter-power spectra with the similar shapes in the k-range where SDSS-DR7 data is present but different amplitudes. The matter power spectrum is of course influenced by the growth of structure within a given gravity model.

We recall again from above that the ISW-effect is dependent on the quantity $(\dot{\phi}+\dot{\psi})^2$, while the weak-lensing signal is dependent on the quantity $\phi+\psi$. Furtheremore, there has been much discussion in previous works [54, 55, 57] as to how different values of the various MG parameters in the various parameterization affect cosmological observations. We will recall some of that discussion related to the growth of structure in order to examine how different MG parameters will affect the matter-power spectrum. In the matter dominated era, the growth of structure (matter overdensities) on sub-horizon scales (but still within the linear regime) is governed by the usual equation $\ddot{\Delta}_m+\mathcal{H}\dot{\Delta}_m+k^2\psi=0$. Super-horizon growth of matter overdensities is a bit more complicated. We refer the reader to eq. (A5) of [55] for a full expression of the growth equation in the matter dominated era ($\mu$ there should not be confused with the $\mu$ in this paper as they are different). As mentioned in the previous reference a $k^2\psi$ term will be present at all scales (it is actually scale-independent through eq. (11)). This term is affected directly by the parameters $\mu$ or $\mathcal{V}$ from the second and third parameterizations respectively, and correspondingly the product of $Q$ and $R$ from the first parameterization. An increase(decrease) in these quantites from their GR values will increase(decrease) the magnitude of the gravitational potential $\psi$. This increase(decrease) in the magnitude of the potential in turn combats(enhances) the suppression of the growth caused by the accelerated expansion of the universe, therebye enhancing(suppressing) the growth relative to its GR value on all scales. This will in turn increase(decrease) the overall amplitude of the matter power spectrum and the weak lensing correlations relative to their GR values. Next, though not explicitly shown in the afforementioned equation for super-horizon growth, the next dominant term in the growth equation on those scales is one involving the derivatives of the potentials. Thus they will involve the derivatives of the MG pararameters (these are shown in the mentioned equation though). In the second parameterization the derivatives don't matter much as they are zero for most of the evolution. For the first parameterization however the derivatives directly involve the parameter $s$ as a multiplicative factor so the parameter $s$ affects the growth on these scales in more ways than just govering how long the gravity modification is effective.

For the second parameterization the effects of the parameters on the matter power spectrum is fairly straight forward. As discussed above an increase(decrease) in $\mu$ will increase(decrease) the overall amplitude of the matter power spectrum. The parameter $\Sigma$ however only affects the low-$k$ matter power spectrum. A $\Sigma>1(\Sigma<1)$ will decrease(increase) the low-$k$ spectra relative to its $\Sigma=1$ value for a given $\mu$. This reflects the low-$k$ suppression(enhancement) of the growth for those parameter values. In the binned form of this parameterization the parameters within a given $k$-bin have the same effects as described above on the spectrum in that $k$-bin, and not affect the other $k$-bin except near the transition between the bins. This allows parameters in different $z$-bins but the same $k$-bin to be degenerate with one another in their effect on the matter power spectrum today. On the other hand, the effect of the first parameterization on the matter power spectrum is a bit more complicated due to the presence of the parameter $s$. As discussed above, just as $\mu$ increases or decreases the amplitude of the matter power spectrum in the second parameterization, the value of the parameter combination $QR$ will increase or decrease the amplitude of the matter power spectrum. How much the amplitude is changed though is affected by the value of $s$. A larger $s$ means that the modification to gravity has not affected growth for very long, and thus the amplitude will be affected minimally. A smaller $s$ on the other hand means the modification has been present for a much longer time and thus the amplitude of the matter power spectrum will be affected most for a smaller $s$. A smaller $s$ will also affect the overall shape of the spectrum, mainly because when $s<1$ gets smaller it allows the modification to affect the evolution of the potential outside of the matter dominated era. For the low-$k$ spectrum as

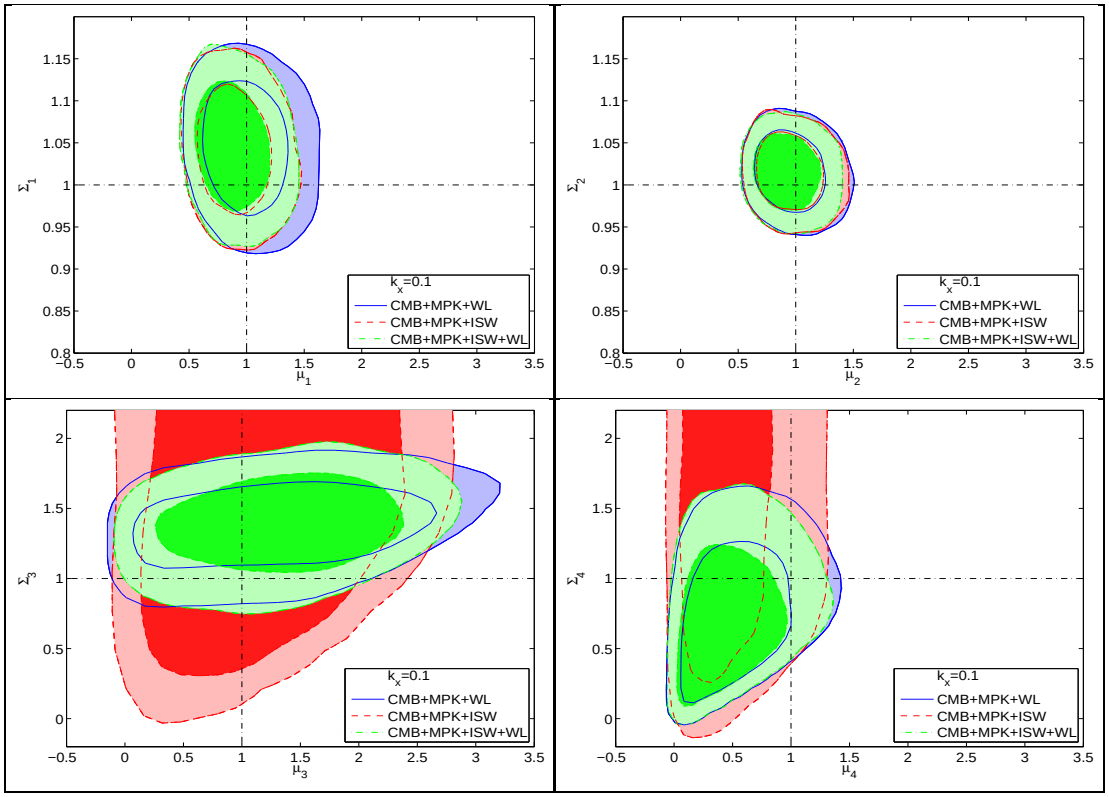


FIG. 5: 68% and 95% C.L. for the parameters $\mu_i$ and $\Sigma_i$ from the second parameterization [57, 68] for redshift and scale dependence as a binned $2 \times 2$ parameterization with $0 < z \leq 1$, $1 < z \leq 2$ and scale separation at $k_x = 0.1\,h\,Mpc^{-1}$. All contours are fit for CMB, MPK, SN, BAO, BBN, AGE and $H_0$. Blue (solid line) contours include WL, red (dashed line) contours include ISW, and green (dashdot line) contours include WL and ISW. The point $(1, 1)$ indicates the GR values.

**with the second parameterization, a $D > 1$ (the parameter corresponding to $\Sigma$) will tend to cause a suppression in the low-$k$ spectrum relative to its $D = 1$ value (the converse still holds for $D < 1$. A larger $s$, however, tends to prefer a suppression in the low-$k$ spectrum and can even overpower the boosting effect of $D < 1$.**

**Independent of parameterization changes to the matter power spectrum will of course affect the other observations such as the weak-lensing correlations, and the ISW-galaxy cross correlations. As discussed in for example [54] values of MG parameters moderately higher than their GR values can lead to an anti-correlation in ISW-galaxy cross correlations at low redshift. Those values of MG parameters promote growth while suppressing the ISW-effect. A more detailed review of the effect of different MG parameters on the ISW-effect in the CMB TT power spectrum is discussed in [54, 55]. Basically both smaller and *sufficiently* larger values of MG parameters compared to their GR values will boost the ISW effect, while values of MG parameters *moderately* larger than their GR values will tend to suppress it. This is because the ISW effect is dependent on the square of $\dot{\phi}+\dot{\psi}$. A smaller/larger value for the MG parameters will increase/decrease $\dot{\phi}+\dot{\psi}$ with larger values even causing the quantity to go negative. For sufficiently large MG parameters though $\dot{\phi}+\dot{\psi}$ will become so negative that the ISW effect is again boosted.**

**The tensions for both parameterizations are possibly due to the way the MG parameters affect the shape and amplitude of the matter power spectrum and the way this change affects the other observables.**

In summary, our results using figures of merits and constraints from current datasets indicate that:

(i) Using the first parameterization with functional form, the strongest current constraints on the MG parameters are found to be from the CMB+ISW+WL combination followed by the CMB+WL or CMB+MPK+ISW.

(ii) We observe, in the case of the first parameterization that the combinations CMB+WL or CMB+MPK does better than CMB+MPK+WL. Similarly, the combinations CMB+ISW+WL or CMB+MPK+ISW does better

than the combination CMB+MPK+ISW+WL. A closer look at the best fit models prefered by each combination of datasets shows that tensions appear between the best fit values for the MG parameters preferred by different datasets and that these tensions are much pronounced when using this parameterization.

(iii) Using the second parameterization or the binning methods, we find that the combination CMB+MPK+ISW of current datasets consistently provides some of the strongest constraints on MG parameters.

(iv) When using the second parameterization or the binning methods, we find that the combination CMB+MPK+ISW+WL provides, at best, only little improvement when compared to the combination CMB+MPK+ISW, again indicating some tension between the datasets. But we find here that the tension between the best fit MG parameters is much less pronounced than in the first parameterization although non-negligible.

(v) In order to investigate these tensions, we fixed the core cosmological parameters and left the MG parameters to vary. In the cases of the second parameterization and the binning methods, the FoM's increase consistently (but only moderately in some cases) when adding a data set, indicating that some of the tension was reduced. A closer look at the best fit MG parameters preferred by different datasets shows that, while reduced, a non-negligible scatter is still present. This explains the only moderate improvements obtained in some cases. This indicates that there are non-negligible tensions intrinsic to the MG parameters preferred by different datasets. Moreover, using the first parameterization and fixing the core cosmological parameters did *not* reduce the strong tensions observed between the MG parameters which seems to suggest that the tensions are exacerbated by the functional form that the first parameterization is imposing on the MG parameters.

(vi) We find that combining current datasets does not improve consistently the uncertainties on the MG parameters due to tensions between the best fit MG parameters preferred by different datasets. Some functional forms imposed by the parameterizations can lead to an exacerbation of these tensions and this point requires further future investigations. It remains of interest to use these datasets separately in order to derive independent constraints on the MG parameters and thus allow one to cross-validate the results.

(vii) Unlike previous work that used a binned parameterization and the CFHTLS lensing data, we do not find a deviation from GR using a similar method but the refined HST-COSMOS data, confirming thus previous claims in those studies that the previous result were likely due to some systematic effect in using CFHTLS lensing data.

(viii) Finally, for all the parameterizations and binning methods used here, we find that the parameter values of general relativity are within the 95% confidence level contours for all dataset combinations.

| **Constraints for** $\{\mu_i,\, \Sigma_i\}$ **binned parameterization** $0 < z \leq 1.5,\, 1.5 < z \leq 3$ | | | |
|---|---|---|---|
| | $k_x = 0.01$ | | |
| Datasets | WL | ISW | ISW, WL |
| $\mathrm{FoM}_1$ | 94.98 | 120.9 | 116.9 |
| $\mu_1$ | [0.629, 1.433] | [0.537, 1.197] | [0.540, 1.222] |
| $\Sigma_1$ | [0.929, 1.127] | [0.948, 1.137] | [0.939, 1.128] |
| $\eta_1$ (derived) | [0.4004, 2.348] | [0.702, 2.992] | [0.659, 2.914] |
| $\mathrm{FoM}_2$ | 149.6 | 165.7 | 163.5 |
| $\mu_2$ | [0.620, 1.455] | [0.570, 1.352] | [0.579, 1.384] |
| $\Sigma_2$ | [0.952, 1.071] | [0.959, 1.074] | [0.956, 1.069] |
| $\eta_2$ (derived) | [0.368, 2.307] | [0.485, 2.616] | [0.433, 2.542] |
| $\mathrm{FoM}_3$ | 28.20 | 40.89 | 46.09 |
| $\mu_3$ | [0.393, 1.807] | [0.594, 1.446] | [0.604, 1.443] |
| $\Sigma_3$ | [0.869, 1.234] | [0.795, 1.209] | [0.862, 1.238] |
| $\eta_3$ (derived) | [0.133, 4.479] | [0.288, 2.489] | [0.387, 2.576] |
| $\mathrm{FoM}_4$ | 48.17 | 68.50 | 69.97 |
| $\mu_4$ | [0.494, 1.600] | [0.545, 1.270] | [0.574, 1.318] |
| $\Sigma_4$ | [0.886, 1.145] | [0.858, 1.133] | [0.879, 1.146] |
| $\eta_4$ (derived) | [0.239, 3.135] | [0.509, 2.687] | [0.483, 2.631] |

TABLE V: 95% C.L. for the parameters $\mu_i$, $\eta_i$, and $\Sigma_i$ from the second parameterization [57, 68] for redshift and scale dependence as a binned $2 \times 2$ parameterization with $0 < z \leq 1.5$, $1.5 < z \leq 3$ and scale separation at $k_x = 0.01\, h\, Mpc^{-1}$. The data used is described in the text above and indicated as: ISW-galaxy cross correlations (ISW), weak lensing tomography (WL). In all cases, the data used is combined with WMAP7 temperature and polarization spectrum (CMB), the matter power spectrum (MPK), SN, BAO, BBN, AGE and $H_0$. The FoM for each dataset and $\{\mu_i,\, \Sigma_i\}$ bin is also given.

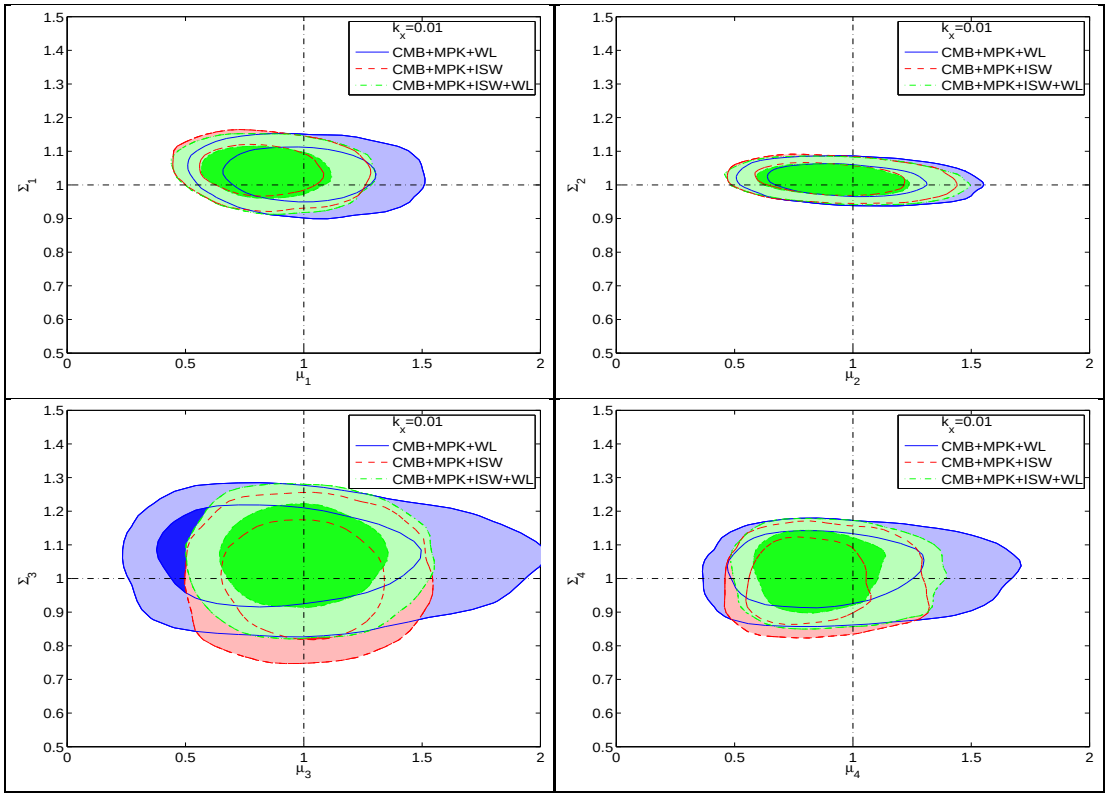


FIG. 6: 68% and 95% C.L. for the parameters $\mu_i$ and $\Sigma_i$ from the second parameterization [57, 68] for redshift and scale dependence as a binned $2 \times 2$ parameterization with $0 < z \leq 1.5$, $1.5 < z \leq 3$ and scale separation at $k_x = 0.01\, h\, Mpc^{-1}$. All contours are fit for CMB, MPK, SN, BAO, BBN, AGE and $H_0$. Blue (solid line) contours include WL, red (dashed line) contours include ISW, and green (dashdot line) contours include WL and ISW. The point $(1, 1)$ indicates the GR values.

**Acknowledgments**

We thank T. Schrabback, G. B. Zhao, R. Bean, E. Linder, I. Tereno, D. Huterer, Y-S. Song, S. Daniel, and P. Zhang for useful comments. We are grateful to G. B. Zhao for making his code `MGCAMB` available to us. `MGCAMB` was modified and used for the second parameterization in this paper while we modified a full separate set of codes that we used for the first parameterization including a new modified version of `CAMB`, `CosmoMC`, as well as WL and ISW codes. The codes that we developed are available from the authors at [89]. M.I. acknowledges that this material is based upon work supported by Department of Energy (DOE) under grant DE-FG02-10ER41310 and that part of the calculations for this work have been performed on the Cosmology Computer Cluster funded by the Hoblitzelle Foundation. J.D. acknowledges that this research was supported in part by an award from DOE Office of Science Graduate Fellowship Program (SCGF). The DOE SCGF Program was made possible in part by the American Recovery and Reinvestment Act of 2009. The DOE SCGF program is administered by the Oak Ridge Institute for Science and Education for the DOE. ORISE is managed by Oak Ridge Associated Universities (ORAU) under DOE contract number DE-AC05-06OR23100. All opinions expressed in this paper are the authors' and do not necessarily reflect the policies and views of DOE, ORAU, or ORISE.

---

[1] A. Lue, R. Scoccimarro, G. Starkman, Phys. Rev. D.**69** 124015 (2004).
[2] Y. S. Song, Phys. Rev. D.**71** 024026 (2005).
[3] L. Knox, Y.S. Song, J. A. Tyson, Phys. Rev. D.**74** 023512 (2005) astro-ph/0503644
[4] M. Ishak, A. Upadhye, D. Spergel, Phys. Rev. D.**74** 043513 (2006). astro-ph/0507184 (astro-ph/0507184);
[5] E. Linder, Phys. Rev. D.**72** 043529 (2005). astro-ph/0507263
[6] T. Koivisto and D. F. Mota, Phys. Rev. D. **73**:083502,(2006).
[7] K. Koyama, JCAP **0603**:017 (2006). astro-ph/0601220
[8] P. Zhang, Phys. Rev. D.**73** 123504 (2006). astro-ph/0511218
[9] P.J. Zhang, M. Liguori, R. Bean, S. Dodelson. Phys.Rev.Lett. **99** 141302 (2007). arXiv:0704.1932
[10] Hu W. and I. Sawicki, Phys. Rev. D **76**, 104043 (2007)
[11] R. Caldwell, A. Cooray, A. Melchiorri, Phys.Rev.D **76**:023507 (2007) astro-ph/0703375
[12] S. Wang, L. Hui, M. May, Z. Haiman, Phys. Rev. D.**76** 063503 (2007) arXiv:0705.0165
[13] M. Kunz, D. Sapone, Phys. Rev. Lett. **98** 121301 (2007). astro-ph/0612452
[14] D. Huterer, E. Linder. Phys. Rev. D.**75** 023519 (2007). astro-ph/0608681
[15] E. Linder, R. Cahn. Astropart. Phys. **28** 481 (2007). astro-ph/0701317
[16] O. Dore et. al, (2007) arXiv: 0712.1599
[17] Y. S. Song, I. Sawicki, W. Hu, Phys. Rev. D.**75** 064003 (2007). astro-ph/0606286
[18] G. Gabadadze and A. Igelsias, Class. quant. Grav. **25** 154008 (2007). arXiv:0712.4086
[19] D. Polarski and R. Gannouji, Phys. Lett. B. **660** 439-443 (2007). arXiv:0710.1510
[20] V. Acquaviva, A. Hajian, D. Spergel, S. Das. Phys. Rev. D.**78** 043514 (2008). arXiv:0803.2236
[21] E. Bertschinger, P. Zukin, Phys. Rev. D **78** 024015 (2008) arXiv:0801.2431
[22] S. Daniel, R. Caldwell, A. Cooray, A. Melchiorri Phys. Rev. D **77** 103513 arXiv:0802.1068
[23] Y. Gong, Phys. Rev. D.**78** 123010 (2008). arXiv:0808.1316
[24] W. Hu, Phys. Rev. D.**77** 103524 (2008). arXiv:0801.2433
[25] B. Jain, P. Zhang, Phys. Rev. D.**78** 063503 (2008). arXiv:0709.2375
[26] H. Wei, N. Zhang, Phys. Rev. D.**78** 023011 (2008). arXiv: 0803.3292
[27] J. Dent, S. Dutta, L. Perivolaropoulos, Phys. Rev. D.**80** 023514 (2009). arXiv:0903.5296
[28] X. Fu, P. Wu, H. Yu, Phys. Lett. B **677** 12-15 (2009). arXiv:0905.1735
[29] Y. Gong, M. Ishak, A. Wang, Phys. Rev. D.**80** 023002 (2009). arXiv:0903.0001
[30] R. Gannouji, B. Moraes, D. Polarski, (2009). arXiv: 0907.0393
[31] M. Ishak, J. Dossett, Phys. Rev. D.**80** 043004 (2009). arXiv:0905.2470
[32] E. Linder, Phys. Rev. D.**79** 063519 (2009), arXiv:0901.0918
[33] P. Serra, A. Cooray, S. Daniel, R. Caldwell, A. Melchiorri, Phys. Rev. D **79** 101301 (2009) arXiv:0901.0917
[34] Y. S. Song, O. Dore, JCAP 0903:025 (2009). arXiv:0812.0002
[35] Y.S. Song, W. Percival, JCAP **0910**:004 (2009). arXiv:0807.0810
[36] S. Thomas, F. Abdalla, J. Weller, MNRAS **395** 197-209 (2009) arXiv:0810.2269
[37] S. Tsujikawa, R. Gannouji, B. Moraes, D. Polarski, Phys. Rev. D.**80** 084044 (2009). arXiv:0908.2269
[38] P. Wu, H. Yu, X. Fu, Phys. Rev. D.**79** 083513 (2009). arXiv:0905:3444
[39] G. Zhao, L. Pogosian, A. Silvestri, J. Zylberberg, Phys. Rev. D **79** 083513 (2009) arXiv:0809.3791
[40] G. Zhao, L. Pogosian, A. Silvestri, J. Zylberberg, Phys. Rev. Lett. **103** 241301 (2009) arXiv:0905.1326
[41] V. Acquaviva, E. Gawiser, Phys. Rev. D.**82** 082001 (2010). arXiv:1008.3392
[42] J. Dossett, M. Ishak, J. Moldenhauer, Y. Gong, A. Wang, JCAP **1004**:002 (2010) arXiv:1004.3086
[43] P. Ferreira, C. Skordis, Phys. Rev. D.**81** 104020 (2010). arXiv:1003.4231

[44] J. Jing, S. Chen, Phys. Lett. B **685** 185 (2010). arXiv:0908.4379
[45] L. Pogosian, A. Sivestri,K. Koyama, G. Zhao, Phys.Rev.D **81**:104023 (2010) arXiv:1002.2382
[46] Y. S. Song, L. Hollenstein, G. Caldera-Cabral, K. Koyama, JCAP **1004**:018 (2010) arXiv:1001.0969
[47] Peebles J., The large scale structure of the universe (Princeton University Press, 1980)
[48] Fry, Phys. Lett. B, **158**, 211 (1985).
[49] Lightman and Schecheter, Astrophys. J. 74, **831**, 1990
[50] Wang and Steinhardt, Astrophys. J 508, **483**, 1998.
[51] Will M.C, Theory and Experiment in Gravitational Physics, ISBN 0 521 43973 (Cambridge, 1993).
[52] Will M. C., The Confrontation between General Relativity and Experiment, Living Rev. Relativity 9, (2006).
[53] S. Daniel, R. Caldwell, A. Cooray, P. Serra, A. Melchiorri, Phys.Rev.D **80**:023532 (2009) arXiv:0901.0919
[54] R. Bean and M. Tangmatitham, Phys. Rev. D **81** 083534 (2010) arXiv:1002.4197
[55] S. Daniel, E. Linder, T. Smith, R. Caldwell, A. Corray, A Leauthaud, L. Lombriser, Phys. Rev. D **80** 123508 (2010) arXiv:1002.1962
[56] S. Daniel and E. Linder Phys.Rev.D **82** 103523 (2010). arXiv:1008.0397
[57] G. Zhao et. al. Phys.Rev.D **81** :103510, (2010) arXiv:1003.0001
[58] L. Lombriser, (2011) arXiv:1101.0594
[59] I. Toreno, E. Semboloni, T. Schrabback (2010) arXiv:1012.5854
[60] B. A. Reid et al. MNRAS Volume **404**, Issue 1, pages 6085, May 2010, arXiv:0907.1659.
[61] W. J. Percival et al. MNRAS Volume **401**, Issue 4, pages 21482168, February 2010, arXiv:0907.1660.
[62] The WMAP team likelihood as compiled by J.Dunkley, E.Komatsu, D.L.Larson, M.R.Nolta, January 2010; http://lambda.gsfc.nasa.gov/; and papers D. Larson et al., (2010), arXiv:1001.4635; N. Jarosik et al., (2010), arXiv:1001.4744; E. Komatsu et al., (2010), arXiv:1001.4538.
[63] R. Amanullah et al., Astrophys. J. **716**, 712 (2010) arXiv:1004.1711.
[64] S. Ho, C. Hirata, N. Padmanabhan, U. Seljak, and N. Bahcall, Phys. Rev. D. **78**, 043519 (2008), 0801.0642.
[65] C. Hirata, S. Ho, N.Padmanabhan, U. Seljak, N. Bahcall, Phys.Rev.D78:043520 (2008), 0801.0644.
[66] T. Schrabback et al. Astronomy and Astrophysics, Volume **516**, A63, (2010), arXiv:0911.0053.
[67] C. Ma and E. Bertshinger, Astrophys. J. **455**, 7 (1995).
[68] Private communication with G.B. Zhao. A previous version of the code is available at: http://userweb.port.ac.uk/~zhaog/MGCAMB.html
[69] A. Albrecht, et. al. Report of Dark Energy Task Force, (2006), astro-ph/0609591.
[70] A. Albrecht, et. al., (2009), [arxiv:0901.0721].
[71] Y. Wang, et. al. (2010), [arxiv:1006.3517].
[72] C. Ma and T. Zhang, (2010), [arxiv:1007.3787].
[73] A. Amara, T. Kitching, (2010), [arxiv:1009.3274].
[74] M. J. Mortonson , D. Huterer, W. Hu, (2010) [arxiv:1004.0236].
[75] M. J. Mortonson, W. Hu and D. Huterer, Phys. Rev. D. **79**, 023004 (2009), [arXiv:0810.1744].
[76] M. J. Mortonson, W. Hu and D. Huterer, Phys. Rev. D. **81**, 063007 (2010), [arXiv:0912.3816].
[77] Y. Wang, Phys. Rev. D. **77**, 123525 (2008), [arXiv:0803.4295].
[78] A.G. Riess *et al.*, Astrophys. J. **659**, 98 (2007).
[79] N. Scoville, R. G. Abraham, H. Aussel, et. al. (2007), ApJS, **172**, 38.
[80] O. Ilbert, P. Capak, M. Salvato, et. al. (2009), ApJ, 690, 1236.
[81] J. Lesgourgues, M. Viel, M.G. Haehnelt, R. Massey, JCAP0711:008 (2007).
[82] A. Lewis, A. Challinor, A. Lasenby, Astrophys. J. **538**, 473 (2000); http://camb.info
[83] A. Lewis and S. Bridle, Phys. Rev. D **66** (2002) 103511.
[84] J. Hartlap, P. Simon, and P. Schneider, (2007), A and A, **464**, 399.
[85] T. Schrabback, private communication.
[86] M. Ishak, Foundation of Physics Journal **37**:1470-1498, (2007). [astro-ph/0504416]
[87] L. Fu, et. al. Astron. Astrophys. **479**:9-25, (2008), [arxiv:0712.0884]
[88] We intended in this work to apply the analysis to the CFHTLS weak lensing data but it was recommended to us by leading members of the CFTLS weak lensing team to wait until the next data release because of known residual systematics in the T003 data release.
[89] The MG versions of the modified codes `CAMB`, `CosmoMC`, ISW code, as well as the HST COSMOS 3D weak lensing likelihood code that we developed, are available upon request from jnd041000@utdallas.edu.